AIP | Review of Scientific Instruments

Non-equilibrium phonon generation and detection in microstructure devices

J. B. Hertzberg, O. O. Otelaja, N. J. Yoshida, and R. D. Robinson

Citation: Rev. Sci. Instrum. **82**, 104905 (2011); doi: 10.1063/1.3652979
View online: http://dx.doi.org/10.1063/1.3652979
View Table of Contents: http://rsi.aip.org/resource/1/RSINAK/v82/i10
Published by the AIP Publishing LLC.

Non-equilibrium phonon generation and detection in microstructure devices

J. B. Hertzberg, O. O. Otelaja, N. J. Yoshida, and R. D. Robinson
Department of Materials Science and Engineering, Cornell University, Ithaca, New York 14853, USA

(Received 30 March 2011; accepted 26 September 2011; published online 31 October 2011)

We demonstrate a method to excite locally a controllable, non-thermal distribution of acoustic phonon modes ranging from 0 to ∼200 GHz in a silicon microstructure, by decay of excited quasiparticle states in an attached superconducting tunnel junction (STJ). The phonons transiting the structure ballistically are detected by a second STJ, allowing comparison of direct with indirect transport pathways. This method may be applied to study how different phonon modes contribute to the thermal conductivity of nanostructures. © *2011 American Institute of Physics*. [doi:10.1063/1.3652979]

Non-equilibrium phonons are an effective means to probe the frequency dependence of phonon transport.[1–5] Existing methods to study thermal transport in dielectric structures permit either (a) spectrally resolved measurements of phonon modes in bulk-size samples,[3,4,6] or (b) measurement of total heat transmission (thermal conductance) in nanoscale samples.[7–11] However, the latter type of measurement cannot distinguish among phonon modes and cannot tell whether the phonons scatter inelastically in transit. In this article, we demonstrate a more precise probe: a microscale source of nonequilbrium phonons exhibiting a sharp edge in its spectral distribution. We adjust the frequency of this edge from 0 to ∼200 GHz by varying the voltage across a superconducting tunnel junction (STJ), and observe the ballistic transmission of phonons of energy $\gtrsim$80 GHz through a silicon microstructure. We describe how future experiments may adapt this technique to measure transmission of selected phonon modes through nanostructures.

At low temperatures, reduced scattering allows acoustic phonons to propagate in a straight line for long distances.[12,13] To create a technique to probe a microstructure with such ballistic phonons, we construct our devices so that the phonon generator and detector face each other across the microstructure (Figure 1(a)), unlike the strictly planar geometry used elsewhere.[14] To do so we introduce several refinements in the fabrication process: We first form "mesa" type microstructures 1.46 μm high by 250 μm long by 30 μm wide on top of a 500 μm thick substrate (Figure 1), using KOH etch (50% KOH, 48 °C, for 9.5 min) of a (100) silicon wafer masked by silicon nitride. The sidewalls of the mesas are smooth (111) planes at a 54.7° angle to the wafer surface. We form the STJs by thin-film deposition of Al, using double-angle shadow evaporation and lift-off of a bilayer of LOR polymer (Microchem Inc.) and S1818 photoresist (Rohm and Haas Inc.).[15,16] The depth-of-field of the photolithographic process enables us to resolve the pattern across the mesa. All devices, wiring traces and bond-pads are formed simultaneously in a simple one-step process, with 12 devices per chip and 112 chips per wafer. The deposited films (70 and 170 nm thick) and intervening tunnel barrier (grown in 6 Torr of oxygen for 26 min) are continuous up the sidewall and onto the mesa top. Any one of the devices may be used as either a phonon generator or detector. When a STJ is used for phonon detection, its Josephson current must first be suppressed. The double-junction geometry (SQUID configuration, Figure 2(a)) enables Josephson current cancellation by a magnetic field applied perpendicular to the plane of the device. The normal state resistances R_n of the STJs used in this study ranged from 774 to 1084 Ω. A typical device appears in Figure 2(a).

Figure 2(b) illustrates our measurement apparatus. The 500 μm thick Si chip holding the devices was clamped to a copper sample stage coated with a film of Apiezon N grease, and the stage was bolted to the cold head of a He-3 refrigerator held at a temperature of 0.3 K. Signals were measured through filtered twisted-pair lines. During each set of measurements, we applied to the phonon generator a fixed ac current modulation $\delta I_{gen} = 15$ to 36 $\mathrm{nA_{RMS}}$, plus a stepped DC current $I_{gen} = -1.5$ to 1.5 μA. To minimize electromagnetic crosstalk, we chose modulation frequencies $\leq$13 Hz . The detector meanwhile was voltage-biased in the "sub-gap" regime at a fixed value of 0.2 mV. To zero the Josephson current, a magnetic field perpendicular to the chip was adjusted between 0.2 and 0.3 G. The steady-state DC detector current was 0.15 to 0.22 nA, which is within 50% of the thermally activated quasiparticle tunneling rate predicted by BCS theory at 0.3 K.[17] The modulated detector current, representing the modulated portion of incident phonon flux, was distinguished by a low-noise preamplifier and lock-in amplifier over a range from ~ -1 to 1 $\mathrm{pA_{RMS}}$. The steady-state detector current also rose by up to 15% in these measurements as I_{gen} was increased to its maximum value. Our sensitivity was limited by noise in our electronics and by electrical pickup noise, which varied somewhat from measurement to measurement. The lowest level of noise we achieved was 100 $\mathrm{fA}/\sqrt{\mathrm{Hz}}$.

Phonon emission energies are controlled by superconducting quasiparticle processes.[1–3,18–20] In the generator, bias voltage V injects quasiparticle excitations into the superconducting film through electron tunneling. Each excitation will have an energy (denoted ϵ_{QP}) within a range from Δ to $eV - \Delta$. Here Δ is the superconducting bandgap of Al, 170 μeV, and energies are referenced to the Fermi level. Within the Al film, the quasiparticles scatter elastically, undergoing diffusive motion. The quasiparticles are also subject to inelastic processes, giving up their energy in two stages.

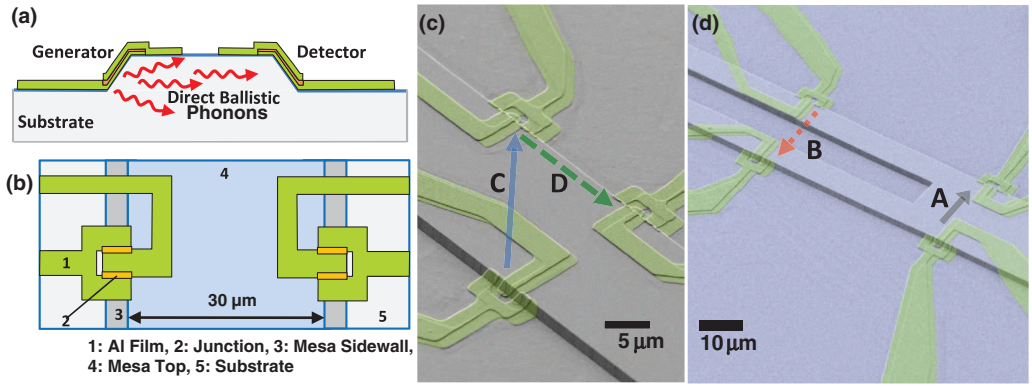

FIG. 1. (Color) (a) Schematic diagram of STJ phonon generator and detector arranged on microscale silicon mesa for direct ballistic phonon measurement. Cross-sectional view through mesa is shown here. (b) Schematic diagram of top view of silicon mesa showing geometry and formation of double-junction (SQUID type) STJs. Individual SQUID appears in detail in Figure 2. (c) and (d) False-colored SEM images of STJ phonon generator-detector pairs (A–D) on opposing sides of silicon mesa 1.46 μm high by 30 μm wide, on top of a 500 μm thick silicon substrate. Each pair is indicated by an arrow pointing from generator to detector: a solid arrow indicating a direct line-of-sight for phonons, a dashed arrow if there is none. Pair B is identical to A except that the ballistic path in B is interrupted by a trench etched into the mesa. The detector STJ in pair C is also used as the generator STJ in pair D. Measurements using these devices (Figure 3) confirm that phonons travel in line-of-sight from generator to detector.

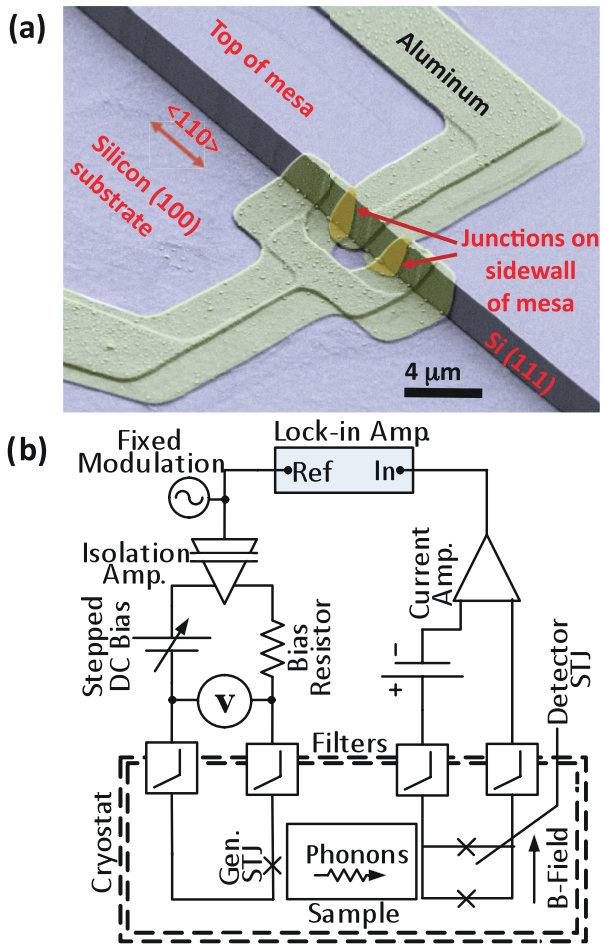

FIG. 2. (Color) (a) False-colored SEM image of double-junction (SQUID type) aluminum STJ deposited onto sidewall of 1.46 μm high Si mesa. (b) Schematic diagram of phonon transport measurement. Sample is held at 0.3 K in a He-3 cryostat. Generator circuitry applies a fixed AC modulation $\delta I_{gen} =$ 15 to 36 nA_{RMS}, plus a stepped DC current $I_{gen} = -1.5$ to 1.5 μA. Detector STJ is held at a fixed magnetic field to suppress Josephson current and held at a fixed 0.2 mV bias. Lock-in amplifier monitors the oscillations in detector tunneling current due to modulated phonon flux.

First, they relax rapidly to the gap-edge, dropping to energy Δ with time scale $\tau_{rel} \sim 1$ ns.[2] The lost energy emerges as phonons having energies ranging from 0 to $eV - 2\Delta$ ("relaxation" phonons). Next, recombination into Cooper pairs annihilates the quasiparticles, again emitting phonons. These "recombination" phonons have energy 2Δ with an emission linewidth governed by thermal effects and other factors. The recombination process has a time scale τ_{rec} that is much longer than τ_{rel} and is strongly dependent on temperature and on the bandgap of the superconductor. At an experimental temperature of 0.3 K, for aluminum having a bandgap of 170 μeV, the decay time should be $\tau_{rec} \sim 30$ μs.[2,21,22] Both longitudinal and transverse phonon modes are expected to emerge from each process.[2]

The excited phonon spectrum is thus highly non-thermal, comprising a nearly monochromatic component of recombination phonons of energy $\sim 2\Delta$, plus a broad distribution of relaxation phonons with a sharp cutoff at $eV - 2\Delta$.[2,18] The STJ radiates these phonons into the adjacent silicon. Because the AC modulation affects only those quasiparticles injected with energy $\epsilon_{QP} \sim eV - \Delta$, it likewise affects only the phonons emitted by these quasiparticles, i.e., the relaxation phonons at the cutoff energy $eV - 2\Delta$ plus the portion of $\sim 2\Delta$ recombination phonons emitted by these same quasiparticles.[2] At the detector meanwhile, the process works somewhat in reverse: any phonons of energy $\geq 2\Delta$ ($\sim$80 GHz) that enter the Al metal may excite quasiparticles. The quasiparticles move diffusively through the film and can decay by recombination; those that reach the junction and tunnel through it constitute the detector signal. The ratio $\delta I_{det}/\delta I_{gen}$ of the modulated detector and generator signals will therefore be[2]

$$\frac{\delta I_{det}}{\delta I_{gen}}(V) = A_g \frac{\Omega}{4\pi} A_{foc} \cdot T_{ac} \cdot n_{gen}(V) \cdot n_{det}. \qquad (1)$$

Here T_{ac} is an acoustic mismatch factor, $T_{ac} = T_{gs} T_{sd} (c_g^2/c_s^2)$, where T_{gs} and T_{sd} are transmission factors for the generator-to-silicon and silicon-to-detector

acoustical impedances, and c_g and c_s are the generator and silicon acoustic speeds. For Al and Si, T_{ac} is ~0.1 averaged over all angles and wave polarizations.[2] Since we expect phonons radiated from the generator into the silicon to travel ballistically, the factor $A_g(\Omega/4\pi)$ is the fraction that we expect to be collected by the detector (Figure 1(a)). (This fraction is adjusted somewhat due to phonon focusing effects in the silicon, as discussed below.) Here A_g is the fraction of generator emission area visible from the detector, and Ω the solid angle subtended by detector collection area relative to generator. The values of A_g and Ω are governed by the geometry and dimensions of the mesa, the generator and the detector. Diffusion of the quasiparticles in both the generator and detector superconducting films is also relevant here. In the generator, tunneled quasiparticles may diffuse away from the junction before decaying and emitting phonons through the relaxation and recombination processes. Because relaxation is a much quicker process than recombination, relaxation phonons will be emitted from only a small region very close to the generator junction, whereas recombination phonons may be emitted from a larger area. From published values of ~20 cm^2/s for the diffusion constant in Al at 0.3 K,[23,24] and assuming $\tau_{rel} \sim 1$ ns and $\tau_{rec} \sim 30$ μs, we estimate the diffusion length for relaxation to be ~1.4 μm and for recombination to be ~250 μm. Relaxation phonons are of greater interest here because they constitute the portion of the emitted phonon spectrum whose energy may be controlled. Since the generator junction lies on the mesa sidewall, a large fraction of the relaxation phonons will be emitted such that they can propagate directly to the detector by line-of-sight. Many of the recombination phonons, however, will be emitted from the wiring traces leading to the generator, having no direct path of propagation to reach the detector. At the detector meanwhile similar issues are relevant. Because of the long diffusion length for quasiparticle recombination, phonons absorbed in detector wiring traces may register as part of the signal. However, in Eq. (1) the factor Ω refers only to the line-of-sight signal. In these devices, some portions of the detector wiring do lie on the mesa top or the mesa sidewall and can therefore contribute to the solid angle Ω (see Figure 1). As described below, we compare direct and indirect phonon transmission geometries in order to subtract off the indirect signal.

In contrast with past work employing STJs to generate and detect non-equilibrium phonon populations, several adaptations in the present work are worth noting. Earlier experiments typically used generator and detector junctions 10 μm to 1 mm in size, deposited onto opposite faces of a crystal several mm in dimension.[2,20] In such work one could assume that all of the generator emission area is visible from the detector, and therefore all generator current contributes to the measurable phonon flux. In contrast, the form of our microfabricated devices necessitates the factor A_g in Eq. (1). The role of quasiparticle diffusion in determining the effective detector area was not typically considered in macroscopic phonon detectors.[25] Although the recombination time τ_{rec} is lower at temperatures closer to the T_c of the superconductor, the diffusion length will always exceed the junction dimensions used here. In the detectors, Josephson current suppression must also be accomplished differently in our devices than in past work. In large tunnel junctions, a magnetic field aligned parallel to the junction may be used, but this is not possible in a smaller device, necessitating the double-junction arrangement used here.

The nondimensional factor A_{foc} in Eq. (1) represents the enhancement (or reduction) of signal intensity due to "phonon focusing" in the direction of propagation between generator and detector.[26–28] In an isotropic medium, this factor is 1, while in a crystal selected "caustic" directions may exhibit several orders of magnitude of enhancement for one or more wave polarization.[28] As indicated in Figure 2, in our devices the line between phonon generator and detector lies within or close to the (100) plane. In silicon the "caustic" directions of the fast-transverse wave polarization lie slightly out of the (100) crystal plane, and will fall within our measurements.[29–31] Assuming that an equal population of each wave polarization is emitted by the generator STJ, we estimate focusing factors from published values of the enhancement in silicon.[27,30,32] The enhancement relative to an isotropic medium should range from ~3 in the (110) direction to ~6 near the (100) direction. The detectors pictured in Figure 1 subtend angles up to 20° in the (100) plane, with greater angular ranges occupied by the wiring traces. In practice, the factor $(\Omega/4\pi)A_{foc}$ in Eq. (1) must therefore be found as an integrated product of the solid angle and focusing factor over the extent of the detector. The somewhat complicated geometry of our devices makes this difficult to calculate precisely.

The remaining factors in Eq. (1) deal with the emitted phonons' frequency distribution. The factor $n_{gen}(V)$ in Eq. (1) is the number of phonons of energy $\geq 2\Delta$ that the generator produces for each tunneled electron, and n_{det} is the number of charges collected in the detector for each entering phonon. Relaxation of excited quasiparticles will produce phonons of energy $\geq 2\Delta$ only if the quasiparticles have energy $\epsilon_{QP} \geq 3\Delta$ above the Fermi level. Thus only at generator voltages $V \geq 4\Delta/e$ will the step-edge in the emitted spectrum of recombination phonons include energies $\geq 2\Delta$.

This behavior is evident in measurements of the devices of Figure 1, appearing in Figure 3. Because the generator is current-biased, its IV characteristic skips over voltages in the high-impedance "subgap" regime, and therefore no data points appear at voltages below $2\Delta/e$. At voltages $2\Delta/e < V < 4\Delta/e$, the generator emits recombination phonons of energy 2Δ, resulting in a constant signal at the detector. The sharp rise in signal at $V = 4\Delta/e$ demonstrates the production of relaxation phonons having energies $\geq 2\Delta$, as well as the ~80 GHz high-pass response of the detector. An ohmic heater biased and modulated in this way, emitting a Bose-Einstein distribution of phonons, is incapable of producing such a response. Preservation of a non-equilibrium phonon spectrum also indicates that phonons do not thermalize in transit between generator and detector.

To confirm direct ballistic transport, we compare different pairs of generators and detectors (Figures 1 and 3 and Table I). Whereas macroscopic phonon transport studies have typically relied on pulse time-of-flight to distinguish direct from indirect paths,[18,19] we instead vary the transport path:

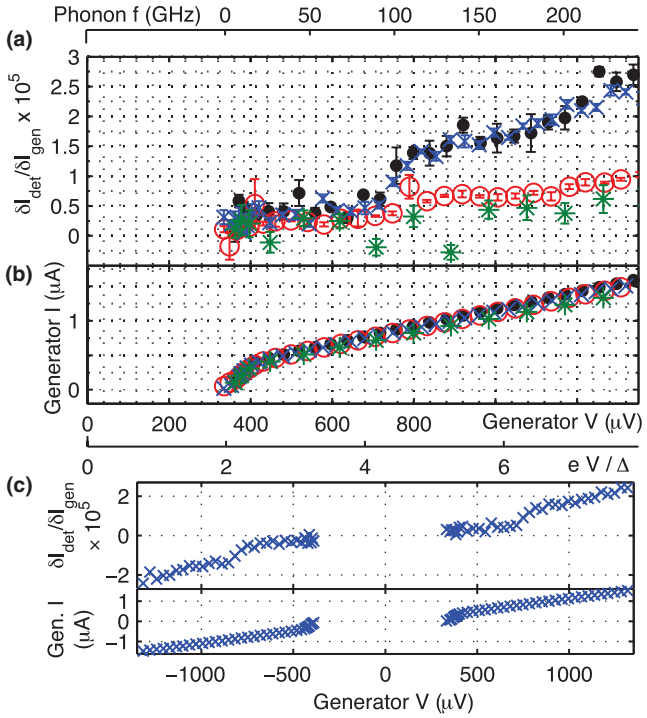

FIG. 3. (Color) Phonon transmission measurements, as a function of generator voltage, for generator/detector pairs shown in Figure 1 and listed in Table I, A (•, black), B (○, red), C (×, blue), D (∗, green). (a) Detectors' response to modulated generator current, while each detector is voltage-biased at 0.2 mV and generator current is stepped. (Error bars are standard error of repeated measurements at same I_{gen}, retaining points within 1.5 standard deviation.) At generator voltage $4\Delta/e$, the step-change in response indicates relaxation phonons of energy $\geq 2\Delta$ emitted by generator. (b) Current through generator STJs during these measurements. Note that all generators behave nearly identically and exhibit no features in the I–V curve at $V = 4\Delta/e$. Plots a and b share a common horizontal scale. In each measurement the generator current I_{gen} was stepped in increments roughly equal to the peak-to-peak current modulation amplitude, so that the resulting voltage increments roughly equal the energy resolution of the measurement. Energy resolution values are listed in Table I. Additional scale above part (a) indicates upper limit of relaxation phonon distribution, and below part (b) restates the generator voltage as a multiple of aluminum bandgap $\Delta = 170$ μeV. (c) Pair C, data scale extended to show both positive and negative generator voltages.

Since generator/detector pair B is identical to pair A except that the direct path through the silicon is blocked by a trench, we can take the pair B signal to represent a "background" or "indirect" signal, and the difference between the pair A signal and the pair B signal to represent strictly the ballistic phonon flux in pair A. In this way we seek to localize the measured signal to only the transmission through the mesa itself. This kind of comparison has also been demonstrated in some macroscopic phonon-transport experiments by sawing slots into bulk crystals, which is more cumbersome than microfabricated etch.[31,32] A similar comparison may be made to pair C.

The presence of a trench in the silicon should not have any effect on electromagnetic crosstalk, so subtracting off the "indirect" signal should also have the benefit of canceling the effect of crosstalk from the measurement. We also note that the signal in pair D, which also lacks a line-of-sight between generator and detector, is as small as in pair B. In pair D, the generator and detector lie on a continuous plane, but the phonons evidently do not travel along this plane. The fact that pair B and pair D exhibit similar signal sizes suggests that "indirect" transmission occurs by a scattering process within the silicon.

As phonon-phonon scattering is negligible at the measurement temperature and isotope scattering in crystalline Si is expected to have a mean free path >10 cm at these phonon frequencies, the most likely explanation is that the phonons are scattering from the bottom of the chip, a ~1 mm round-trip.[32] The long quasiparticle diffusion lengths in the aluminum films mean that a flux of scattered phonons traveling upward within the chip may be intercepted by the detector wiring leads and register as a signal at the detector. Within a distance roughly equal to the diffusion length for quasiparticle recombination (~250 μm) these wiring traces cover an area of about 10^4 square microns on top of the substrate. We note that the transmitted signal for pair B appears to exhibit a step at $V = 4\Delta/e$ (Figure 3(a)). This behavior may be worth exploring more closely in future measurements. Such a step would indicate that despite a ~1 mm round-trip and scattering from the bottom of the chip, the phonons have not thermalized. The mean free path of phonons at this temperature through silicon has been shown to be $\gg 1$ mm.[12] The devices employed here were fabricated from standard single-side-polished Si wafer, and no special precautions were made to thermalize the rear side of the chip, other than clamping it to the sample stage on a film of thermally conducting grease. In future experiments it may be possible to reduce the indirect signal by using thicker substrates, or amorphous substrates for which the phonon mean free path is shorter than the substrate thickness, or by coating the back side of the chips with a metal or some other material that may help thermalize incident phonons.

The factors $T_{ac} \cdot n_{gen}(V) \cdot n_{det}$ in Eq. (1) represent the combined efficiency of phonon generation and detection. For direct phonon transmission, we quantify this in the regime where the signal should be due primarily to relaxation phonons. For each measurement, we average the signal between generator voltages of $4\Delta/e$ and $6\Delta/e$, and report these values in Table I. Subtracting the indirect signal level and dividing out geometric and phonon-focusing factors $A_g(\Omega/4\pi)A_{foc}$, we find efficiencies 0.2% for pair A and 0.7% for pair C. These values, similar to the 1% levels seen in macroscopic experiments,[18] appear to represent roughly equal contributions from acoustic mismatch ($T_{ac} \simeq 0.1$) and losses within the superconducting films of both generator and detector. A variety of processes within the superconductor can affect n_{gen} and n_{det}.[22] In the detector, quasiparticle recombination and outdiffusion into the leads compete with tunneling to diminish n_{det}, while on the other hand "quasiparticle trapping" in a confined region of the detector may enhance it by effectively extending the recombination lifetime τ_{rec}. To improve the efficiency of the phonon transmission measurement in future experiments, these processes must be more carefully controlled.

Figure 3 also illuminates other processes at play in this system. Because phonons of energy $>2\Delta$ within the generator may suffer reabsorption, at $V > 4\Delta/e$ fewer phonons will occupy the spectral edge $eV - 2\Delta$.[2] At $V = 6\Delta/e$, the rise in signal suggests that high-energy quasiparticles emit multiple relaxation phonons, increasing n_{gen}. We have also observed

TABLE I. Summary of the device geometries shown in Figure 1 and measurements made using these devices (Fig. 3). Phonon generators and detectors are attached to silicon mesas 1.46 μm high by 30 μm wide, on the top surface of a 500 μm thick silicon chip. The last column lists the average magnitude of $\delta I_{det}/\delta I_{gen}$ for the regime expected to be dominated by generator 'relaxation' phonons, i.e., generator voltages $|4\Delta/e| < V < |6\Delta/e|$.

Generator/ detector pair	Line-of-sight	Geometry	Calculated $A_g(\Omega/4\pi)A_{foc}$	modulation δI_{gen} (nA_{RMS})	Energy resolution (μeV)	Avg. signal $\delta I_{det}/\delta I_{gen} \times 10^5$
A	Yes	Facing	3.4×10^{-3}	20.5	48	1.2 ± 0.2
B	No	Blocked by trench	–	20.4	50	0.61 ± 0.03
C	Yes	Facing at angle	1.4×10^{-3}	15.3	36	1.6 ± 0.1
D	No	Side-by-side	–	35.6	91	0.53 ± 0.02

nearly identical response for either positive or negative generator bias (Figure 3(c)), suggesting that even quasiparticles injected into the Al film that is not adjacent to the silicon do emit phonons into the silicon, consistent with a diffusion length >1 μm for quasiparticle relaxation.

Figure 3 also illuminates the related experimental issues of electromagnetic crosstalk between generator and detector, and the energy resolution possible with this technique. In our measurements of phonon transmission through a microstructure, the modulated current through the phonon detector is typically more than 90 dB below the modulation amplitude at the phonon generator. To avoid interfering with the measurement, any crosstalk due to capacitive or inductive coupling from the generator should be made much smaller than this level. To avoid capacitive crosstalk, we restricted the modulation frequencies to values below 13 Hz. To check the crosstalk magnitude, we repeated our measurements at a temperature of 4.2 K, well above the T_c of aluminum, using generator/detector pair A (Figure 1) with generator and detector reversed. At the higher temperature, quasiparticle excitation and decay processes in the metal films will be absent, meaning that there will be no phonon generation and detection, but any capacitive and inductive coupling should persist. The impedance of the generator STJ, which in the superconducting state is biased above the bandgap, will be roughly the same in both cases, although the detector impedance will be lower at the higher temperature. In the measurement at 4.2 K we stepped the generator current I_{gen} through a range −2 to 2 μA, while applying a generator modulation $\delta I_{gen} = 300$ nA_{RMS}. Because the detector in the normal state passes significant DC currents, we reduced the detector bias to 0.05 mV compared to the superconducting case. We applied no magnetic field. In these conditions the magnitude of $\delta I_{det}/\delta I_{gen}$ showed no dependence on generator voltage and had an average magnitude of $(3.1 \pm 0.6) \times 10^{-6}$. This result indicates that crosstalk contributes negligibly to the direct phonon transmission signals (pairs A and C in Figure 3 and Table I), although it may contribute somewhat to the indirect signals. The energy resolution of the measurement is a related issue. The energy resolution comprises the range of generator voltages swept out by the modulation, or $2\sqrt{2}R_n \cdot \delta I_{gen}$ in units of eV. At the modulation frequencies we employed in order to limit crosstalk, instrument noise levels restricted us to use generator modulation amplitudes δI_{gen} greater than 15 nA_{RMS}. Thus in these measurements the smallest energy resolution achieved was 36 μeV (~9 GHz). At zero generator bias current, the crosstalk was more severe, probably due to the very high generator impedance at sub-gap voltages. Data points at zero generator bias are omitted from Figure 3.

In summary, we have demonstrated a micron-scale generator of a non-thermal distribution of phonons whose frequencies are tunable from 0 to ~200 GHz, and detected these at frequencies above ~80 GHz transiting ballistically through a 30 μm silicon microstructure. Successfully adapting STJ-based phonon generation and detection techniques to the microscale has required several methods not used in previous macroscopic efforts, in particular the use of microphotolithography to place STJs onto microstructure sidewalls, the use of double-junction detectors for Josephson-current suppression, and the accounting for the role of quasiparticle diffusion in determining the effective area of the generator and detector. Phonons of controllable energy are emitted by the phonon generators from an area smaller than the phonon emission area of pulsed laser methods[6,33] and comparable to that demonstrated using scanning electron-beams.[34] This spatial resolution may be readily improved by fabricating smaller STJs. Further design improvements could include reducing the mesa width and relocating detector wiring traces. Suspending the devices on a membrane or narrow support wires would add considerably to the complexity of the fabrication, but could be implemented if necessary to further isolate the generator, detector and phonon transmission path. The ability to emit and detect controllable nonthermal phonon spectra, as described here, thus constitutes a prototype for a microfabricated "phonon spectrometer" suitable for the study of phonon transport through nanostructures.[1,2] While some past STJ-based studies explored phonon bandgaps in simple 1-dimensional superlattices,[5] we suggest that in the geometry demonstrated here a variety of nanostructures may be introduced by interposing them into the ballistic path, either by etching them into a silicon mesa or fixing them into a trench such as appears in Figure 1(c). Resonant scattering impurities may also be introduced into the phonon path in the crystal to serve as spectral reference points.[2,19,20] We expect that these techniques will prove useful in exploring surface and interface scattering behavior in nanostructures, and the investigation of phonon transmission across interfaces,[4,12,35] thereby addressing questions about phonon transport through nanostructures that thermal conductance measurements have been unable to resolve.[9] The ability to

easily fabricate many phonon transducers on-chip should aid in the study of these complicated phenomena by facilitating comparison between various nanostructures along with reference measurements.

ACKNOWLEDGMENTS

The authors thank R. B. Van Dover, J. Blakely, S. Baker, K. Schwab, and Cornell LASSP for loan of key equipment, and L. Spietz for photolithography recipes. We thank R. B. Van Dover, K. Schwab, E. Smith, J. Parpia, D. Ralph, B. Plourde, M. Blencowe, D. Westly, R. Pohl, P. Berberich, and C. Mellor for helpful discussions and thank D. Toledo, J. Chang and A. Lin for help with apparatus. The authors acknowledge funding from the National Science Foundation (NSF) (DMR 0520404) and Department of Energy (DOE) (DE-SC0001086). This publication is based on work supported in part by Award No. KUS-C1-018-02, made by King Abdullah University of Science and Technology (KAUST). This work was performed in part at the Cornell NanoScale Facility, a member of the National Nanotechnology Infrastructure Network, which is supported by the National Science Foundation (Grant ECS-0335765).

[1]H. Kinder, Phys. Rev. Lett. **28**, 1564 (1972).
[2]W. Eisenmenger, "Superconducting tunnel junctions as phonon generators and detectors," in *Physical Acoustics – Principles and Methods* (Academic, New York, 1976), pp. 79–153.
[3]W. E. Bron, Rep. Prog. Phys. **43**, 301 (1980).
[4]M. N. Wybourne and J. K. Wigmore, Rep. Prog. Phys. **51**, 923 (1988).
[5]O. Koblinger, J. Mebert, E. Dittrich, S. Döttinger, W. Eisenmenger, P. V. Santos, and L. Ley, Phys. Rev. B **35**, 9372 (1987).
[6]Y.-C. Wen, J.-H. Sun, C. Dais, D. Grützmacher, T.-T. Wu, J.-W. Shi, and C.-K. Sun, Appl. Phys. Lett. **96**, 123113 (2010).
[7]J. S. Heron, T. Fournier, N. Mingo, and O. Bourgeois, Nano Lett **9**, 1861 (2009).
[8]K. Schwab, E. A. Henriksen, J. M. Worlock, and M. L. Roukes, Nature (London) **404**, 974 (2000).
[9]A. I. Hochbaum, R. Chen, R. D. Delgado, W. Liang, E. C. Garnett, M. Najarian, A. Majumdar, and P. Yang, Nature (London) **451**, 163 (2008).
[10]K. Hippalgaonkar, B. Huang, R. Chen, K. Sawyer, P. Ercius, and A. Majumdar, Nano Lett. **10**, 4341 (2010).
[11]J. H. Seol, I. Jo, A. L. Moore, L. Lindsay, Z. H. Aitken, M. T. Pettes, X. Li, Z. Yao, R. Huang, D. Broido, N. Mingo, R. S. Ruoff, and L. Shi, Science **328**, 213 (2010).
[12]T. Klitsner and R. Pohl, Phys. Rev. B **36**, 6551 (1987).
[13]R. J. von Gutfeld and A. H. Nethercot, Phys. Rev. Lett. **12**, 641 (1964).
[14]C. Yung, D. Schmidt, and A. Cleland, Appl. Phys. Lett. **81**, 31 (2002).
[15]L. Spietz, K. Lehnert, I. Siddiqi, and R. Schoelkopf, Science **300**, 1929 (2003).
[16]G. Dolan, Appl. Phys. Lett. **31**, 337 (1977).
[17]T. Van Duzer and C. W. Turner, *Principles of Superconductive Devices and Circuits* (Elsevier, New York, 1981).
[18]W. Eisenmenger and A. H. Dayem, Phys. Rev. Lett. **18**, 125 (1967).
[19]P. Berberich and M. Schwarte, Z. Phys. B: Condens. Matter **64**, 1 (1986).
[20]H. Kinder, Z. Phys. **262**, 295 (1973).
[21]L. Solymar, *Superconductive Tunnelling and Applications* (Chapman and Hall, London, 1972).
[22]C. M. Wilson and D. E. Prober, Phys. Rev. B **69**, 094524 (2004).
[23]V. Savu, L. Frunzio, and D. E. Prober, IEEE Trans. Appl. Supercond. **17**, 324 (2007).
[24]S. Hsieh and J. Levine, Phys. Rev. Lett. **20**, 1502 (1968).
[25]W. Rothmund, C. W. Hagen, and A. Zehnder, Physica B **169**, 447 (1991).
[26]B. Taylor, H. J. Maris, and C. Elbaum, Phys. Rev. Lett. **23**, 416 (1969).
[27]H. Maris, J. Acoust. Soc. Am. **50**, 812 (1971).
[28]J. P. Wolfe, *Imaging Phonons: Acoustic Wave Propagation in Solids* (Cambridge University Press, Cambridge, England, U.K./New York, 1998).
[29]Y. P. Joshi, Solid State Commun. **45**, 455 (1983).
[30]F. Rösch and O. Weis, Z. Phys. B: Condens. Matter **25**, 115 (1976).
[31]J. A. Shields, J. P. Wolfe, and S.-I. Tamura, Z. Phys. B: Condens. Matter **76**, 295 (1989).
[32]S. Tamura, J. A. Shields, and J. P. Wolfe, Phys. Rev. B **44**, 3001 (1991).
[33]S. Zhang, E. Peronne, L. Belliard, S. Vincent, and B. Perrin, J. Appl. Phys. **109**, 033507 (2011).
[34]W. Klein, E. Held, and R. P. Huebener, Z. Phys. B: Condens. Matter **69**, 69 (1987).
[35]F. Rösch and O. Weis, Z. Phys. B: Condens. Matter **27**, 33 (1977).